Scattering and diffraction of plane P and SV waves by two-dimensional inhomogeneities: Part II

Nasser Moeen-Vaziri and Mihailo D. Trifunac

Dept. of Civil Engineering, University of Southern California, University Park, Los Angeles, CA 90089-1114, USA

The scattering the diffraction of plane P and SV waves by two dimensional inhomogeneities have been studied. A least-squares technique has been employed to solve the problem. The results are obtained using the series expansion in terms of Bessel and Hankel functions. The method is then applied to idealized cross sections along profiles of Los Angeles basin, California, to investigate the effects of subsurface inhomogeneities on scattering and diffraction of plane longitudinal P, and transverse SV waves. The surface displacement amplitudes and displacement amplitudes along buried horizontal lines are also discussed.

1. INTRODUCTION

Detailed understanding of the effects of wave scattering and diffraction through geological inhomogeneities is of obvious value to earthquake engineering and strong motion seismology. For studies of the effects of inhomogeneities smaller than the wavelengths and for waves with long periods, simple models seem to be satisfactory. However, there are many cases in strong motion seismology and earthquake engineering where near field ground motions should be considered, in which the waves with shorter periods become important.

In many recent earthquake damage studies the evidence of strong and localized wave amplification has been observed. Hudson[1] showed that the influence of irregular geological structure or topography may overshadow the effects of local site conditions. The study by Gutenberg[2] indicates that the sites with softer alluvium yield higher amplitudes and longer durations than the 'stiffer' sites, and the intensity of ground shaking can vary within a short distance.

The model studied by Sezawa[3] is an example of an early formulation of elastic wave scattering applicable to strong motion seismology. He investigated the scattering and diffraction of elastic waves by embedded rigid circular and elliptical cylinders in an elastic full space. The review by Miklowitz[4] indicates that there have been numerous efforts to investigate the diffraction of elastic waves by obstacles of different geometries following Sezawa's work.

There has been a considerable amount of work on scattering of plane SH waves (e.g., Aki and Larner[5]; Bard and Bouchon[6]; England et al.[7]; Lee and Trifunac[8]; Moeen-Vaziri and Trifunac[9-11]; Sabina and Willis[12]; Sanchez-Sesma and Esquivel[13]; Sanchez-Sesma and Rosenblueth[14]; Sanchez-Sesma et al.[15]; Sills[16]; Trifunac[17,18]; Wong and Jennings[19]; Wong and Trifunac[20,21]; Wong et al.[22]) because for the two-dimensional inhomogeneities this problem is governed by the scalar wave equation and its solution is thus relatively

simple. There has been some research done on scattering and diffraction of elastic waves involving the plane strain models as well. However, the complexity of the plane strain models is greater when compared to the antiplane strain models. This is mainly due to the mode conversion during reflection and transmission, which does not permit one to use the method of images, and the coupled longitudinal and shear wave components at the free surface.

Cisternas et al.[23] presented a theoretical analysis of body waves in a 'real earth'. Bouchon and Aki[24] described a method to study the radiation and scattering near a seismic source in an irregular layered medium. Using a Green's function method, Mal and Knopoff[25] studied the propagation of Rayleigh waves past a step change in the elevation of the surface of a homogeneous half-space. Wang and Hermann[26] published a solution for the surface displacements due to buried dislocation sources in a multi-layered elastic medium. Bouchon[27] employed the method developed by Aki and Larner[5] to investigate the effects of different topographic features on surface motion. A generalized inverse method was developed by Wong[28] to study the diffractions of P, SV and Rayleigh waves by surface irregularities. Dravinski[29] studied the influence of interface depth of ground motion. He also used a boundary integral method (Dravinski[30]) to investigate the amplification of P, SV and Rayleigh waves by two arbitrary shaped alluvial valleys.

A few researchers used the perturbation methods to study the effects of minor irregularities on wave amplification (e.g., McIvor[31]; Asano[32]; Suteau and Martel[33]). Due to complicated mathematical analysis, these methods are not always practical for engineering applications.

There are very few analyses carried out for elastic wave scattering by three-dimensional obstacles. With an acoustic approximation, Singh and Sabina[34] obtained the exact solution for a hemispherical cavity subjected to incident P waves. However, such an approximation can be applied in very few cases. Lee[35] analysed scattering and diffraction of P, SV and SH waves by a hemispherical

canyon in an elastic half-space. Wong[36] and Wong and Luco[37] studied the wave scattering problems involving surface obstacles. Lee and Trifunac[38] studied body wave excitation of embedded hemispheres. Sanchez-Sesma[39] applied a boundary method to solve the scattering and diffraction of elastic waves by axisymmetric three dimensional surface irregularities.

The objective of this study is to investigate the effects of subsurface inhomogeneities and irregularities of arbitrary shape on the ground motion amplification. The numerical applications made in this presentation centre around P and SV waves. The method of analysis used in this work is mainly an extension of the work done by Sanchez-Sesma[39], on diffraction of elastic waves by three dimensional surface irregularities, and Moeen-Vaziri and Trifunac[10], on scattering of plane SH-waves by cylindrical canals of arbitrary shape.

1.1 Wave equation in polar coordinates

For the model considered in this work, the polar coordinate system is suitable for use. Let the function f be of the form $f = f(r, \theta, t)$. The wave equation

$$c^2 \nabla^2 f - \frac{\partial^2 f}{\partial t^2} = 0 \qquad (1.2.1)$$

in polar coordinates is then

$$\frac{\partial^2 f}{\partial r^2} + \frac{1}{r} \frac{\partial f}{\partial r} + \frac{1}{r^2} \frac{\partial^2 f}{\partial \theta^2} = \frac{1}{c^2} \frac{\partial^2 f}{\partial t^2} \qquad (1.2.2)$$

where c is the wave velocity.

Since an arbitrary time variation of the function can be represented by Fourier analysis in terms of harmonic functions, there will be no loss of generality in considering only the harmonic solution of the form

$$f(r, \theta, t) = F(r, \theta) e^{i\omega t} \qquad (1.2.3)$$

where $i = \sqrt{-1}$, ω is the circular frequency and F satisfies the Helmholtz equation

$$\nabla^2 F + K^2 F = 0 \qquad (1.2.4)$$

in which $K = \omega/c$ is the wave number.

By using the method of separation of variables with $F = R(r)\Theta(\theta)$ equation (1.2.4) separates into

$$r^2 R'' + rR' + (K^2 r^2 - p^2)R = 0 \qquad (1.2.5)$$

$$\Theta'' + p^2 \Theta = 0 \qquad (1.2.6)$$

where p is the separation constant. The solutions for $\Theta(\theta)$ are

$$\Theta = e^{\pm ip\theta} \quad \text{or} \quad \begin{pmatrix} \sin p\theta \\ \cos p\theta \end{pmatrix} \qquad (1.2.7)$$

For most problems of interest, Θ must be single valued, i.e., $\Theta(\theta + 2\pi) = \Theta(\theta)$, which requires $p = n$, where n in an integer. Equation (1.2.5) then becomes

$$r^2 R'' + rR' + (K^2 r^2 - n^2)R = 0 \qquad (1.2.8)$$

with the solution that can be expressed in terms of either

Bessel functions of the first and second kind, $J_n(Kr)$ and $Y_n(Kr)$ respectively, or in terms of Hankel functions of the first and second kind, $H_n^{(1)}(Kr)$ and $H_n^{(2)}(Kr)$.

Therefore, let the general solution of equation (1.2.8) be of the form $X_n^{(m)}(Kr)$, $m = 1, 2, 3, 4$, defined as follows:

$$X_n^{(1)} = J_n(Kr)$$

$$X_n^{(2)} = Y_n(Kr)$$

$$X_n^{(3)} = H_n^{(1)}(Kr)$$

$$X_n^{(4)} = H_n^{(2)}(Kr) \qquad (1.2.9)$$

Then the general solution of the wave equation (1.2.2) is any linear combination of two of

$$X_n^{(m)}(Kr) \frac{\sin n\theta}{\cos n\theta} \exp(i\omega t) \qquad (1.2.10)$$

with $m = 1, 2, 3, 4$, and $n = 0, 1, 2, \ldots$.

The two dimensional model studied in this work is shown in Fig. 1. It represents a layered half space $(y > 0)$ with each layer having arbitrary shape. The soil and alluvium are assumed to be elastic and linear, and the contact between the layers is assumed to be welded. The material property of the jth layer is given by Lamé constants λ_j and μ_j, and mass density ρ_j, $j = 1, 2, 3, \ldots$, NL, for which we have

longitudinal wave velocity: $\quad \alpha_j = \sqrt{\dfrac{\lambda_j + 2\mu_j}{\rho_j}}$

and

transverse wave velocity: $\quad \beta_j = \sqrt{\dfrac{\mu_j}{\rho_j}} \qquad (1.2.11)$

NL is the total number of layers. The characteristic horizontal linear dimension of each layer is defined by $2a_j$, $j = 1, 2, 3, \ldots, NL$.

Three coordinate systems are introduced. The rectangular coordinate system with positive x pointing to the right and positive y pointing down. The cylindrical coordinate system, consisting of the radial distance r and
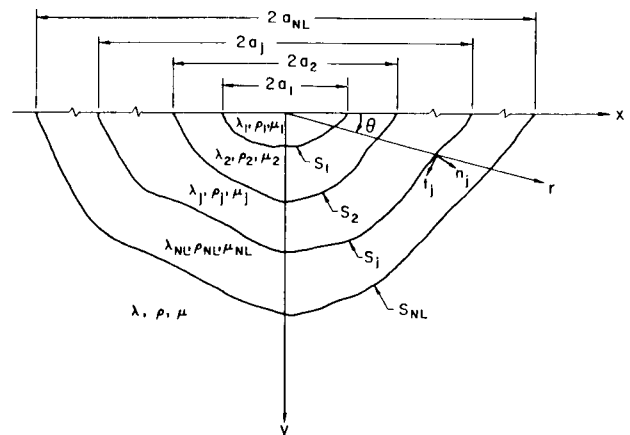

Fig. 1. The Model

the angle θ, measured from the positive x coordinate has a common origin with the rectangular system. Finally, the normal-tangential local coordinate system (n_j, t_j), is employed which consists of the outward normal n_j to the outer boundary of layer $j, j = 1, 2, \ldots, NL$, and the tangent to this boundary t_j (Fig. 1).

2. EXCITATION: INCIDENT P-WAVE

The excitation of the half-space is assumed to consist of a plane longitudinal (P) wave with frequency ω. Its displacement vector and propagation vector are situated in the x-y plane. It can be represented by the potential

$$\phi^{(i)} = \frac{1}{h} \exp i\omega \left(t - \frac{x}{C_{px}} + \frac{y}{C_{py}} \right) \qquad (2.1.1)$$

For an incident angle δ, measured relative to the x-axis, the phase velocities along the x-axis, C_{px}, and y-axis, C_{py}, are given by (see Fig. 2)

$$C_{px} = \frac{\alpha}{\cos \delta} \qquad C_{py} = \frac{\alpha}{\sin \delta} \qquad (2.1.2)$$

where α is the longitudinal wave velocity in the half-space and $h = \omega/\alpha$ is the longitudinal wave number.

Far from the inhomogeneity, (Fig. 1), the incident waves are reflected from the free surface ($y = 0$). The incident P-waves generate both plane reflected longitudinal (P) and transverse (SV) waves, with their potentials given by

(reflected P-wave): $\quad \phi^{(r)} = \dfrac{A_1}{h} \exp i\omega \left(t - \dfrac{x}{C_{px}} - \dfrac{y}{C_{py}} \right)$

$$(2.1.3)$$

(reflected SV-wave): $\quad \psi^{(r)} = \dfrac{A_2}{h} \exp i\omega \left(t - \dfrac{x}{C_{sx}} - \dfrac{y}{C_{sy}} \right)$

$$(2.1.4)$$

where A_1 and A_2 are reflection coefficients defined by (Achenbach[40])

$$A_1 = \frac{\sin 2\delta \sin 2\gamma - \left(\dfrac{\alpha}{\beta} \right)^2 \cos^2 2\gamma}{\sin 2\delta \sin 2\gamma + \left(\dfrac{\alpha}{\beta} \right)^2 \cos^2 2\gamma} \qquad (2.1.5)$$
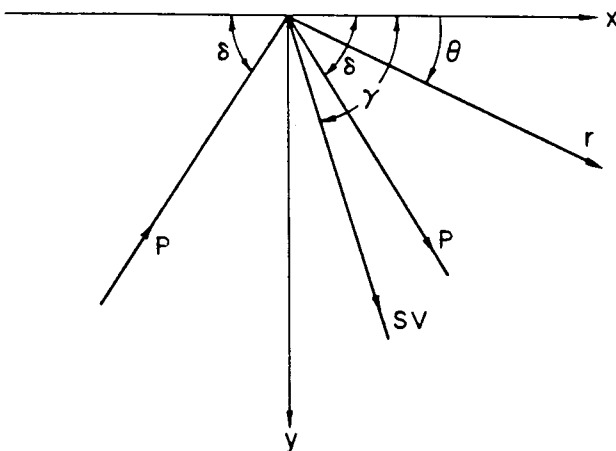

Fig. 2.   Incident P-*wave*

and

$$A_2 = \frac{-2 \left(\dfrac{\alpha}{\beta} \right) \sin 2\delta \cos 2\gamma}{\sin 2\delta \sin 2\gamma + \left(\dfrac{\alpha}{\beta} \right)^2 \cos^2 2\gamma} \qquad (2.1.6)$$

C_{sx} and C_{sy} are the phase velocities of SV waves along x and y axes and γ is their incidence angle, β is the transverse wave velocity in the half space. The relationship between the incident angles of longitudinal and transverse incident waves is given by

$$\cos \gamma = \kappa^{-1} \cos \delta \qquad (2.1.7)$$

in which $\kappa = \alpha/\beta$ is the material constant

$$\kappa = \left[\frac{2(1 - v)}{1 - 2v} \right]^{1/2}$$

with v being the Poisson ratio of the half-space.

Equations (2.1.1), (2.1.3) and (2.1.4) can be rewritten as (Pao and Mow[41])

$$\phi^{(i)} = \frac{1}{h} \sum_{n=0}^{\infty} d_n (-i)^n J_n(hr) \cos n(\theta + \delta) \qquad (2.1.9)$$

$$\phi^{(r)} = \frac{A_1}{h} \sum_{n=0}^{\infty} d_n (-i)^n J_n(hr) \cos n(\theta - \gamma) \qquad (2.1.10)$$

$$\psi^{(r)} = \frac{A_2}{h} \sum_{n=0}^{\infty} d_n (-i)^n J_n(Kr) \cos n(\theta - \gamma) \qquad (2.1.11)$$

where $h = \omega/\alpha$ and $K = \omega/\beta$ are the longitudinal and transverse wave numbers and d_n is defined as

$$d_n = \begin{cases} 1 & \text{for } n = 0 \\ 2 & \text{for } n \geqslant 1 \end{cases}$$

and the time factor $\exp(\omega t)$ is understood.

In the presence of the layered medium, incident $\phi^{(i)}$ and waves $\phi^{(r)}$ and $\psi^{(r)}$ reflect from the surface $y = 0$, and are scattered and diffracted, in the vicinity of the last layer, by the outer boundary of this layer, S_{NL} (Fig. 1). These new longitudinal (P) and transverse (SV) waves are given by the potentials $\phi^{(R)}$ and $\psi^{(R)}$. The resultant free-field potentials are then

$$\phi^{ff} = \phi^{(i)} + \phi^{(r)} + \phi^{(R)} \qquad (2.1.12)$$

$$\psi^{ff} = \psi^{(r)} + \psi^{(R)} \qquad (2.1.13)$$

The waves are also refracted into each layer. The motion in each layer consists of longitudinal (P) and transverse (SV) waves. These waves are denoted by the potentials ϕ^{f_j} and ψ^{f_j} respectively, $j = 1, 2, \ldots, NL$.

2.1 Boundary conditions

The resulting potentials ϕ^{ff}, ψ^{ff}, ϕ^{f_j} and ψ^{f_j} must satisfy the differential equation (1.2.2) for $j = 1, 2, \ldots, NL$. The displacements and stresses corresponding to these potentials, namely $u_n^{ff}, u_t^{ff}, \sigma_{nn}^{ff}, \sigma_{nt}^{ff}, \sigma_{r\theta}^{ff}, \sigma_{\theta\theta}^{ff}, u_n^{f_j}, u_t^{f_j}, \sigma_{nn}^{f_j}, \sigma_{nt}^{f_j}, \sigma_{r\theta}^{f_j}$ and $\sigma_{\theta\theta}^{f_j}$ must satisfy the following boundary conditions:

(1) Stress free condition on the half-space surface

First layer $\qquad \sigma_{r\theta}=0,\ \sigma_{\theta\theta}=0$
at $\theta=0$ and $\theta=\pi$ and r *in the first layer*

$$\vdots$$

*j*th layer $\qquad \sigma_{r\theta}=0,\ \sigma_{\theta\theta}=0$
at $\theta=0$ and $\theta=\pi$ and r in the *j*th layer for $j=1,2,\ldots,$ $NL-1$

$$(2.2.1)$$

half-space layer $\qquad \sigma_{r\theta}=0,\ \sigma_{\theta\theta}=0$

at $\theta=0$ and $\theta=\pi$ and r in the half-space

$$(2.2.2)$$

(2) Continuity of displacements

$$\begin{aligned} u_n^{f_j}&=u_n^{f_{j+1}}\\ u_t^{f_j}&=u_t^{f_{j+1}} \end{aligned}\quad \text{on } S_j,\qquad j=1,2,\ldots,NL-1 \qquad (2.2.3)$$

$$u_n^{f_{NL}}=u_n^{ff}$$

$$u_t^{f_{NL}}=u_t^{ff}\qquad \text{on } S_{NL}\qquad (2.2.4)$$

(3) Continuity of stresses

$$\begin{aligned} \sigma_{nn}^{f_j}&=\sigma_{nn}^{f_{j+1}}\\ \sigma_{nt}^{f_j}&=\sigma_{nt}^{f_{j+1}} \end{aligned}\quad S_j,\qquad j=1,2,\ldots,NL-1 \qquad (2.2.5)$$

$$\sigma_{nn}^{f_{NL}}=\sigma_{nn}^{ff}$$

$$\sigma_{nt}^{f_{NL}}=\sigma_{nt}^{ff}\qquad \text{on } S_{NL}\qquad (2.2.6)$$

In which (n,t) are the normal and tangential coordinates as shown in Fig. 1. $2a_j$ is the total width of the *j*th layer.

Equations (2.2.1) through (2.2.5) represent the boundary conditions to be applied in the calculation of the potentials $\phi^{(R)}$, $\psi^{(R)}$, ϕ^{f_j} and ψ^{f_j}. Once these potentials are known, the free-field displacement and the displacement in each layer can be determined.

2.2 Solution of the problem

The procedure for solving this problem is similar to what has been done for plane *SH*-wave problem by Moeen-Vaziri and Trifunac[11]. Unlike *SH*-waves, the diffraction of *P*-waves is coupled with *SV*-waves, making the problem mathematically and physically more difficult to solve. Consider the sets of linearly independent and not necessarily orthogonal functions:

$$\begin{aligned} &_jQ_n^{(1)}(\mathbf{x}) \qquad _jQ_n^{(2)}(\mathbf{x}) \qquad n=0,1,2,3,\ldots\\ &_jR_n^{(1)}(\mathbf{x}) \qquad _jR_n^{(2)}(\mathbf{x}) \qquad j=1,2,\ldots,NL \end{aligned}\qquad (2.3.1)$$

and

$$T_n(\mathbf{x})\qquad V_n(\mathbf{x})\qquad n=0,1,2,3,\ldots \qquad (2.3.2)$$

that have the following properties:

(i) Each T_n is a solution of the partial differential equation (1.2.2) in the free-field region and $_jQ_n^{(1)}$ and $_jQ_n^{(2)}$ are solutions of the same differential equation in *j*th layer, with $C=\beta$ in (1.2.2).

(ii) Each V_n is a solution of equation (1.2.2) in the free-field region and $_jR_n^{(1)}$ and $_jR_n^{(2)}$ are solutions of this equation in the *j*th layer, with $C=\alpha$ in (1.2.2).

(iii) T_n and V_n satisfy the Sommerfeld's outward radiation condition at infinity.

Next one can assume the following series expansions for the potential functions:

$$\phi^{f_1}=\frac{1}{h}\sum_{n=0}^{N}\{_1Q_n^{(1)}(\mathbf{x})[_1a_n\sin n\theta+{}_1b_n\cos n\theta]$$
$$+\,_1Q_n^{(2)}(\mathbf{x})[_1c_n\sin n\theta+{}_1d_n\cos n\theta]\}$$

$$\psi^{f_1}=\frac{1}{h}\sum_{n=0}^{N}\{_1R_n^{(1)}(\mathbf{x})[_1A_n\sin n\theta+{}_1B_n\cos n\theta]$$
$$+\,_1R_n^{(2)}(\mathbf{x})[_1C_n\sin n\theta+{}_1D_n\cos n\theta]\}$$

$$\phi^{f_2}=\frac{1}{h}\sum_{n=0}^{N}\{_2Q_n^{(1)}(\mathbf{x})[_2a_n\sin n\theta+{}_2b_n\cos n\theta]$$
$$+\,_2Q_n^{(2)}(\mathbf{x})[_2c_n\sin n\theta+{}_2d_n\cos n\theta]\}$$

$$\psi^{f_2}=\frac{1}{h}\sum_{n=0}^{N}\{_2R_n^{(1)}(\mathbf{x})[_2A_n\sin n\theta+{}_2B_n\cos s\theta]$$
$$+\,_2R_n^{(2)}(\mathbf{x})[_2C_n\sin n\theta+{}_2D_n\cos n\theta]\}$$

$$(2.3.3)$$

$$\vdots \qquad\qquad \vdots$$

$$\phi^{f_j}=\frac{1}{h}\sum_{n=0}^{N}\{_jQ_n^{(1)}(\mathbf{x})[_ja_n\sin n\theta+{}_jb_n\cos n\theta]$$
$$+\,_jQ_n^{(2)}(\mathbf{x})[_jc_n\sin n\theta+{}_jd_n\cos n\theta]\}$$

$$\psi^{f_j}=\frac{1}{h}\sum_{n=0}^{N}\{_jR_n^{(1)}(\mathbf{x})[_jA_n\sin n\theta+{}_jB_n\cos n\theta]$$
$$+\,_jR_n^{(2)}(\mathbf{x})[_jC_n\sin n\theta+{}_jD_n\cos n\theta]\}$$

$$\vdots \qquad\qquad \vdots$$

$$\phi^{f_{NL}}=\frac{1}{h}\sum_{n=0}^{N}\{_{NL}Q_n^{(1)}(\mathbf{x})[_{NL}a_n\sin n\theta+{}_{NL}b_n\cos n\theta]$$
$$+\,_{NL}Q_n^{(2)}(\mathbf{x})[_{NL}c_n\sin n\theta+{}_{NL}d_n\cos n\theta]\}$$

$$\psi^{f_{NL}}=\frac{1}{h}\sum_{n=0}^{N}\{_{NL}R_n^{(1)}(\mathbf{x})[_{NL}A_n\sin n\theta+{}_{NL}B_n\cos n\theta]$$
$$+\,_{NL}R_n^{(2)}(\mathbf{x})[_{NL}C_n\sin n\theta+{}_{NL}D_n\cos n\theta]\}$$

$$\phi^{R}=\frac{1}{h}\sum_{n=0}^{N}T_n(\mathbf{x})[e_n\sin n\theta+f_n\cos n\theta]$$

$$\psi^{R}=\frac{1}{h}\sum_{n=0}^{N}V_n(\mathbf{x})[E_n\sin n\theta+F_n\cos n\theta]\qquad (2.3.4)$$

Due to the linear character of the properties (i) through (iii), ϕ^R, ϕ^{f_j}, ϕ^R and ψ^{f_j}, $j=1,2,\ldots,NL$, for $n=0,1,2,3,\ldots,N$ also satisfy them. It can be seen (Moeen-Vaziri and Trifunac[11]) that the stresses derived from the potentials in equations (2.1.9), (2.1.10) and (2.1.11) satisfy the boundary condition (2.2.2), therefore the boundary conditions (2.2.1) and (2.2.2) must be satisfied the stresses

derived from potentials ϕ^{f_j}, ψ^{f_j}, ϕ^R and ψ^R respectively. Furthermore, the displacements and the stresses derived from these potentials must satisfy the boundary conditions listed in equations (2.2.3), (2.2.4), (2.2.5) and (2.2.6). Applying these conditions at different points taken on the plane free surface and on the irregular boundaries would give rise to the following equations:

$$\sigma_{r\theta}^{(\phi^{f}{}_1)}(g_1^{l_1}) + \sigma_{r\theta}^{(\psi^{f}{}_1)}(g_1^{l_1}) = 0$$

at $\theta = 0$ and $\theta = \pi$ and r in the first layer

$$\sigma_{\theta\theta}^{(\phi^{f}{}_1)}(g_1^{l_1}) + \sigma_{\theta\theta}^{(\psi^{f}{}_1)})(g_1^{l_1}) = 0$$

$$u_n^{(\phi^{f}{}_1)}(S_1^{k_1}) + u_n^{(\psi^{f}{}_1)})(S_1^{k_1}) - u_n^{(\phi^{f}{}_2)}(S_1^{k_1}) - u_n^{(\psi^{f}{}_2)}(S_1^{k_1}) = 0$$

$$u_t^{(\phi^{f}{}_1)}(S_1^{k_1}) + u_t^{(\psi^{f}{}_1)}(S_1^{k_1}) - u_t^{(\phi^{f}{}_2)}(S_1^{k_1}) - u_t^{(\psi^{f}{}_2)}(S_1^{k_1}) = 0$$

$$\text{on } S_1$$

$$\sigma_{nn}^{(\phi^{f}{}_1)}(S_1^{k_1}) + \sigma_{nn}^{(\psi^{f}{}_1)}(S_1^{k_1}) - \sigma_{nn}^{(\phi^{f}{}_2)}(S_1^{k_1}) - \sigma_{nn}^{(\psi^{f}{}_2)}(S_1^{k_1}) = 0$$

$$\sigma_{nt}^{(\phi^{f}{}_1)}(S_1^{k_1}) + \sigma^{(\psi^{f}{}_1)}(S_1^{k_1}) - \sigma_{nt}^{(\phi^{f}{}_2)}(S_1^{k_1}) - \sigma^{(\psi^{f}{}_2)}(S_1^{k_1}) = 0$$

$$\vdots$$

$$\sigma_{r\theta}^{(\phi^{f}{}_j)}(g_j^{l_j}) + \sigma_{r\theta}^{(\psi^{f}{}_j)}(g_j^{l_j}) = 0$$

$$\sigma_{\theta\theta}^{(\phi^{f}{}_j)}(g_j^{l_j}) + \sigma_{\theta\theta}^{(\psi^{f}{}_j)}(g_j^{l_j}) = 0$$

at $\theta = 0$ and $\theta = \pi$ and r in the jth layer

$$u_n^{(\phi^{f}{}_j)}(S_j^{k_j}) + u_n^{(\psi^{f}{}_j)}(S_j^{k_j}) - u_n^{(\phi^{f}{}_{j+1})}(S_j^{k_j}) - u_n^{(\psi^{f}{}_{j+1})}(S_j^{k_j}) = 0$$

$$u_t^{(\phi^{f}{}_j)}(S_j^{k_j}) + u_t^{(\psi^{f}{}_j)}(S_j^{k_j}) - u_t^{(\phi^{f}{}_{j+1})}(S_j^{k_j}) - u_t^{(\psi^{f}{}_{j+1})}(S_j^{k_j}) = 0$$

$$\text{on } S_j$$

$$\sigma_{nn}^{(\phi^{f}{}_j)}(S_j^{k_j}) + \sigma_{nn}^{(\psi^{f}{}_j)}(S_j^{k_j}) - \sigma_{nn}^{(\phi^{f}{}_{j+1})}(S_j^{k_j}) - \sigma_{nn}^{(\psi^{f}{}_{j+1})}(S_j^{k_j}) = 0$$

$$\sigma_{nt}^{(\phi^{f}{}_j)}(S_j^{k_j}) + \sigma_{nt}^{(\psi^{f}{}_j)}(S_j^{k_j}) - \sigma_{nt}^{(\phi^{f}{}_{j+1})}(S_j^{k_j}) - \sigma_{nt}^{(\psi^{f}{}_{j+1})}(S_j^{k_j}) = 0$$

$$\sigma_{r\theta}^{(\phi^{f}{}_{NL})}(g_{NL}^{l_{NL}}) + \sigma_{r\theta}^{(\psi^{f}{}_{NL})}(g_{NL}^{l_{NL}}) = 0$$

at $\theta = 0$ and $\theta = \pi$ and r in the half-space

$$\sigma_{\theta\theta}^{(\phi^{f}{}_{NL})}(g_{NL}^{l_{NL}}) + \sigma_{\theta\theta}^{(\psi^{f}{}_{NL})}(g_{NL}^{l_{NL}}) = 0$$

$$u_n^{(\phi^{f}{}_{NL})}(S_{NL}^{k_{NL}}) + u_n^{(\psi^{f}{}_{NL})}(S_{NL}^{k_{NL}}) = u_n^{ff}(S_{NL}^{k_{NL}})$$

$$u_t^{(\phi^{f}{}_{NL})}(S_{NL}^{k_{NL}}) + u_t^{(\psi^{f}{}_{NL})}(S_{NL}^{k_{NL}}) = u_t^{ff}(S_{NL}^{k_{NL}})$$

$$\text{on } S_{NL}$$

$$\sigma_{nn}^{(\phi^{f}{}_{NL})}(S_{NL}^{k_{NL}}) + \sigma_{nn}^{(\psi^{f}{}_{NL})}(S_{NL}^{k_{NL}}) = u_{nn}^{ff}(S_{NL}^{k_{KL}})$$

$$\sigma_{nt}^{(\phi^{f}{}_{NL})}(S_{NL}^{k_{NL}}) + \sigma_{nt}^{(\psi^{f}{}_{NL})}(S_{NL}^{k_{NL}}) = u_{nt}^{ff}(S_{NL}^{k_{NL}}) \quad (2.3.5)$$

In which $j = 1, 2, \ldots, NL$, is the number of layers, $l_j = 1, 2, 3, \ldots, L_j$, is the number of points employed on the free surface of the jth layer and $k_j = 1, 2, 3, \ldots, M_j$ is the number of points used to apply the boundary conditions on the outer boundary of the jth layer. $g_j^{l_j}$ and $S_j^{k_j}$ represent the arguments of the functions at points l_j and k_j of the jth layer.

The system of equations formed by (2.3.5) is a linear

system in terms of complex constants $_ja_n$, $_jb_n$, $_jc_n$, $_jd_n$, $_jA_n$, $_jB_n$, $_jC_n$, $_jD_n$, e_n, f_n, E_n and F_n and can be written as:

$$[A]\{C\} = \{F\} \quad (2.3.6)$$

The row dimension of the coefficient matrix $[A]$, q, is the number of equations used. For each layer j, there are $2L_j$ equations for the flat surface of the half space and $4M_j$ equations for the irregular boundary of the layer. The total number of equations is then

$$q = \sum_{j=1}^{NL} (\text{total number of layers}) \times (2L_j + 4M_j)$$

The column dimension of $[A]$, r, represents the total number of unknowns, which is

$$r = 8 \times (\text{number of terms in each series})$$
$$\times (\text{total number of layers})$$

As it can be seen, in this case one is dealing with much larger matrix dimensions than in the case of the SH-wave problem discussed in Moeen-Vaziri and Trifunac[11]. The vectors $\{C\}$ and $\{F\}$ are $(r \times 1)$ and $(q \times 1)$ respectively. The solution of this overdetermined linear system, in a least-square sense, can be obtained by applying the method of singular value decomposition (Moeen-Vaziri and Trifunac[11]). Once the solution vector $\{C\}$ is determined, the potentials ϕ^{f_j}, ψ^{f_j}, ϕ^R and ψ^R are defined and so are the displacements everywhere in the medium.

To proceed further, the functions $_jQ_n^{(1)}$, $_jQ_n^{(2)}$, $_jR_n^{(1)}$, $_jR_n^{(2)}$, T_n and V_n must be described in detail. The description for these functions can be given by

$$_jQ_n^{(1)} = H_n^{(1)}(h_jr) \qquad _jQ_n^{(2)} = H_n^{(2)}(h_jr)$$
$$j = 2, 3, \ldots, NL$$
$$_jR_n^{(1)} = H_n^{(1)}(K_jr) \qquad _jR_n^{(2)} = H_n^{(2)}(K_jr) \quad (2.3.7)$$

in the first layer:

$$_1Q_n^{(1)} \equiv {}_1Q_n^{(2)} = J_n(h_1r)$$
$$_1R_n^{(1)} \equiv {}_1R_n^{(2)} = J_n(K_1r) \quad (2.3.8)$$

and in the half-space

$$T_n = H_n^{(2)}(hr)$$
$$V_n = H_n^{(2)}(Kr) \quad (2.3.9)$$

in which the functions $J_p(\cdot)$, $H_p^{(1)}(\cdot)$ and $H_p^{(2)}(\cdot)$ are the Bessel function of the first kind and Hankel's functions of the first and second kind respectively.

2.3 Excitation: Incident SV-wave

The analysis for an incident SV wave is similar to the foregoing analysis. The displacement and propagation vectors of the plane SV-wave are situated in the x–y plane. It has angle of incidence γ, circular frequency ω and can be represented by the potential (Fig. 3)

$$\psi^{(i)} = \frac{1}{K} \exp i\omega \left(t - \frac{x}{C_{sx}} + \frac{y}{C_{sy}} \right) \quad (2.4.1)$$

where $K = \omega/\beta$ is the transverse wave number in the half-space.

Fig. 3. Incident SV-wave

Far from the layered medium, the incident waves are reflected from the free surface ($y = 0$). Two different cases are to be considered:

(a) incidence at or beyond the critical angle ($\gamma \geqslant \gamma_{cr}$), and
(b) incidence below the critical angle ($\gamma < \gamma_{cr}$), where the crticial angle, γ_{cr}, is given by

$$\gamma_{cr} = \cos^{-1}(\beta/\alpha) \qquad (2.4.2)$$

Case (a): Incidence at or beyond the critical angle ($\gamma \geqslant \gamma_{cr}$)

Far from the layered inhomogeneity, reflection of incident waves from the free surface ($y = 0$) will generally lead to both longitudinal (P) and transverse (SV) waves, with potentials given by

(reflected P-wave): $\phi^{(r)} = \dfrac{A_1}{K} \exp i\omega\left(t - \dfrac{x}{C_{px}} - \dfrac{y}{C_{py}}\right)$

$$\qquad (2.4.3)$$

(reflected SV-wave): $\psi^{(r)} = \dfrac{A_2}{K} \exp i\omega\left(t - \dfrac{x}{C_{sx}} - \dfrac{y}{C_{sy}}\right)$

$$\qquad (2.4.4)$$

where the reflection coefficients are given by (Achenbach[40])

$$A_1 = \dfrac{\left(\dfrac{\alpha}{\beta}\right)\sin 4\gamma}{\sin 2\gamma \sin 2\delta + \left(\dfrac{\alpha}{\beta}\right)^2 \cos^2 2\gamma} \qquad (2.4.5)$$

and

$$A_2 = \dfrac{\sin 2\gamma \sin 2\delta - \left(\dfrac{\alpha}{\beta}\right)^2 \cos^2 2\gamma}{\sin 2\gamma \sin 2\delta + \left(\dfrac{\alpha}{\beta}\right)^2 \cos^2 2\gamma} \qquad (2.4.6)$$

with

$$\cos \delta = \kappa \cos \gamma \qquad (2.4.7)$$

C_{px}, C_{py} and κ are given by equations (2.1.2) and (2.1.8) respectively. δ is the angle of reflected plane P-waves.

Equations (2.4.1), (2.4.3) and (2.4.4) can be represented by (Pao and Mow[41])

$$\psi^{(i)} = \dfrac{1}{K} \sum_{n=0}^{\infty} d_n(-i)^n J_n(Kr) \cos n(\theta + \gamma) \qquad (2.4.8)$$

$$\phi^{(r)} = \dfrac{A_1}{K} \sum_{n=0}^{\infty} d_n(-i)^n J_n(hr) \cos n(\theta - \gamma) \qquad (2.4.9)$$

$$\psi^{(r)} = \dfrac{A_2}{K} \sum_{n=0}^{\infty} d_n(-i)^n J_n(Kr) \cos n(\theta - \gamma) \qquad (2.4.10)$$

where d_n is defined in section 2.1, and the time factor $\exp(i\omega t)$ is understood.

Case (b): Incidence below the critical angle ($\gamma < \gamma_{cr}$)

In this case, the reflected waves take the form:

$$\phi^{(r)} = \dfrac{A_1}{K} \sum_{n=0}^{\infty} d_n(-i)^n J_n(hr)[C_{n\delta} \cos n\theta + S_{n\delta} \sin n\theta]$$

$$\psi^{(r)} = \dfrac{A_2}{K} \sum_{n=0}^{\infty} d_n(-i)^n J_n(Kr) \cos n(\theta - \gamma) \qquad (2.4.11)$$

where

$$A_1 = \dfrac{\sin 4\gamma}{[\kappa^2 \cos^4 2\gamma + 4(\kappa^2 \cos^2 \gamma - 1)\sin^2 2\gamma \cos^2 \gamma]^{1/2}}$$

$$\times \exp(-i\xi') \qquad (2.4.12)$$

$$A_2 = -\exp(-2i\xi') \qquad (2.4.13)$$

$$\tan \xi' = \dfrac{2(\kappa^2 \cos^2 \gamma - 1)^{1/2} \sin 2\gamma \cos \gamma}{\kappa \cos^2 2\gamma} \qquad (2.4.14)$$

Since in this case, $\cos \delta = \kappa \cos \gamma > 1$ and $\sin \delta$ is imaginary

$$\sin \delta = -i\kappa\xi$$

$$\xi = (\cos^2 \gamma - \kappa^{-2})^{1/2} \qquad (2.4.15)$$

The $C_{n\delta}$ and $S_{n\delta}$ in (2.411), corresponding to the cosine and sine of a complex angle, can be easily evaluated.

The reflected P-wave is a wave propagating in the x direction with wave number $\kappa \cos \gamma$ and phase velocity $\alpha/\kappa \cos \gamma$. The amplitude of the reflected P-wave decays exponentially with distance from the surface.

In both cases (a) and (b), the longitudinal and transverse waves scattered and diffracted near the inhomogeneous medium are defined by potentials $\phi^{(R)}$ and $\psi^{(R)}$ respectively. The motion in each layer is defined by ϕ^j and ψ^j for plane P and SV waves, respectively, $j = 1, 2, \ldots, NL$. The resulting potentials in the half-space are then given by

$$\phi^{ff} = \phi^{(r)} + \phi^{(R)} \qquad (2.4.16)$$

$$\psi^{ff} = \psi^{(i)} + \psi^{(r)} + \psi^{(R)} \qquad (2.4.17)$$

The boundary conditions of the problem for incident plane SV-wave are exactly the same as the conditions given for the case of the plane P-wave in section 2.2, nemely, equations (2.2.1) through (2.2.6). The solution in

this case can be obtained in a similar manner as for the longitudinal case. Following the analysis of section 2.3 the potentials in each layer can be represented by

$$\phi^{f_j} = \frac{1}{K} \sum_{n=0}^{\infty} \{ {}_jQ_n^{(1)}(\mathbf{x})[{}_ja_n \sin n\theta + {}_jb_n \cos n\theta]$$

$$+ {}_jQ_n^{(2)}(\mathbf{x})[{}_jc_n \sin n\theta + {}_jd_n \cos n\theta]\}$$

$$\psi^{f_j} = \frac{1}{K} \sum_{n=0}^{\infty} \{ {}_jR_n^{(1)}(\mathbf{x})[{}_jA_n \sin n\theta + {}_jB_n \cos n\theta]$$

$$+ {}_jR_n^{(2)}(\mathbf{x})[{}_jC_n \sin n\theta + {}_jD_n \cos n\theta]\}$$

$$j = 1, 2, \ldots, NL \qquad (2.4.18)$$

and in the half-space by

$$\phi^{(R)} = \frac{1}{K} \sum_{n=0}^{\infty} T_n(\mathbf{x})[e_n \sin n\theta + f_n \cos n\theta]$$

$$\psi^{(R)} = \frac{1}{K} \sum_{n=0}^{\infty} V_n(\mathbf{x})[E_n \sin n\theta + F_n \cos n\theta] \qquad (2.4.19)$$

where the functions ${}_jQ_n^{(1)}$, ${}_jQ_n^{(2)}$, ${}_jR_n^{(1)}$, ${}_jR_n^{(2)}$, T_n and V_n are defined in section 2.3.

By applying the boundary conditions (2.2.1) through (2.2.6) one can obtain the system of linear equations similar to equation (2.3.6). This sytem can be solved again using the method of singular value decomposition.

2.3.1 Displacement amplitudes

The wave numbers K_j and h_j, and the rigidities μ_j, $j = 1, 2, \ldots$, NL, have been normalized with respect to the corresponding parameters of the half-space K, h, and μ. All the distances have been normalized with respect to the half-width of the first layer, a_1.

For the incident P and SV waves, the moduli of displacement amplitudes are

$$|u_x| = \{[R_e(u_x)]^2 + [Im(u_x)]^2\}^{1/2}$$

$$|u_y| = \{[R_e(u_y)]^2 + [I_m(u_y)]^2\}^{1/2} \qquad (2.4.20)$$

In the absence of the inhomogeneities, the amplitudes of ground displacement in uniform half-space are $|u_x^{ff}|$ and $|u_y^{ff}|$.

The amplitudes given by equations (2.4.20) depend on: (1) the angle of incidence of the plane waves, (2) their frequency, (3) the shear wave velocities β and β_j, (4) the longitudinal wave velocities α and α_j, (5) the Lamé constants μ, λ, μ_j and λ_j, and (6) the geometrical shape and size of the inhomogeneities.

The dimensionless frequency factor, $\eta = 2a_1/l$, where l is the wavelength of incident waves is used to present the numerical results in this paper.

2.4 Comparison with known solutions

If the accuracy of the proposed approximate method could be shown to be adequate for a wide range of frequencies, the method could be applied with confidence to study the diffraction patterns of P and SV waves by two dimensional inhomogeneities. Unlike for the incident SH waves, there are no exact solutions known to the authors, suitable for comparison in this case. Simple comparisons can be performed with the results reviewed by Trifunac[42]

for a uniform half-space and with some of the approximate solutions.

A single layer model with circular boundary and with the material properties of the layer the same as in the surrounding half-space has been used to construct a solution and test it against the known results in a uniform half-space. Figs 4 and 5 present the horizontal and vertical surface displacement amplitudes against the angles of incidence δ and γ for incident P and SV waves respectively. These amplitudes are obtained at point far from the edge of the layer, $x/a_1 = 3.0$, with Poisson's ratio $v = 0.3$ and for $\eta = 0.05$. The results shown in these figures are in agreement with those presented by Trifunac[42].

Next a deep elliptical alluvial valley with major to minor axis ratio, R, equal to 0.4 was used to compare the results, for a different number of terms (5, 7, 9, 11) employed in the series of equations (2.3.4) and (2.3.5). The nature of convergence can be studied by increasing the number of terms as seen in Fig. 6.

There are some approximate solutions in the literature dealing with this problem, which utilize the finite number of line sources to represent the diffracted and scattered fields. However, unfortunately such results are often influenced by the nonunique placement of the sources, by the number of the sources, and by the number of observation points, where the solutions are matched (often in the least squares sense), so that it is difficult to assert their accuracy (e.g., see Wong[28]).
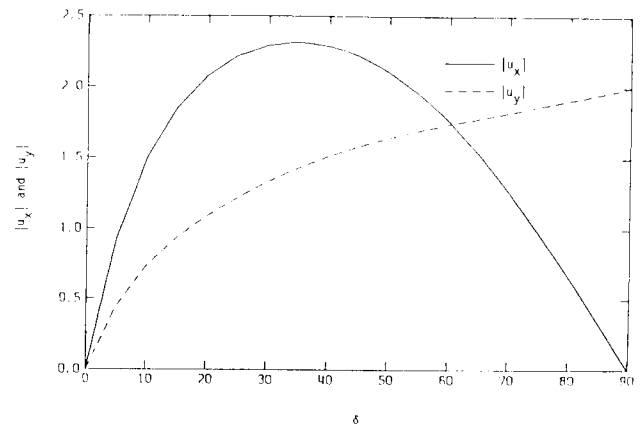

Fig. 4. Horizontal and vertical displacement amplitudes for a uniform half-space model for incident P-waves $(v = 0.3)$
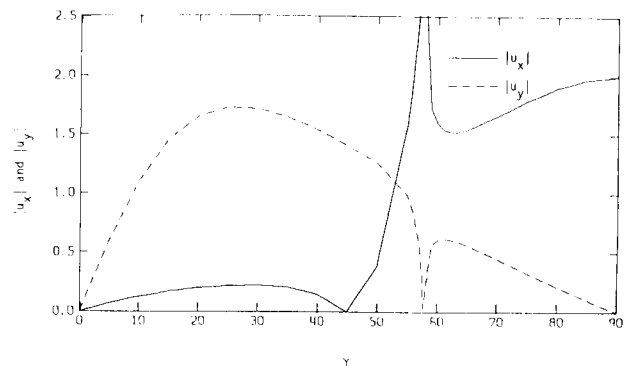

Fig. 5. Horizontal and vertical displacement amplitudes for a uniform half-space model for incident SV-waves $(v = 0.3)$
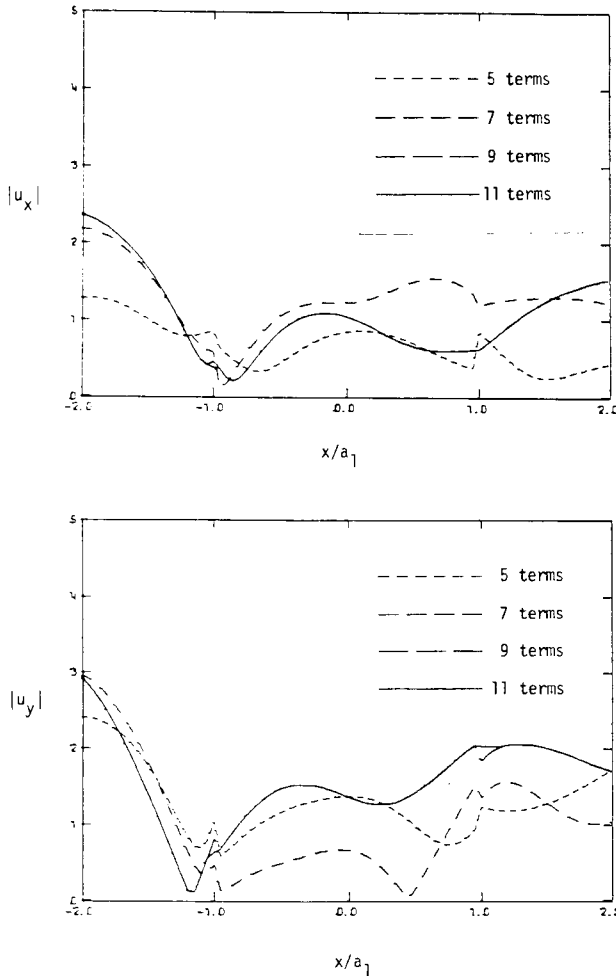
Fig. 6. Horizontal (top) and vertical (bottom) surface displacement amplitudes for a deep elliptical alluvial valley and for incident P-waves with different number of terms in the series ($\delta = 60°$, $\eta = 0.8$, $K_1/K = 1.25$, $h_1/h = 1.25$, $\mu_1/\mu = 0.8$, $R = 0.4$)

2.5 Application to practical geometries

Next the scattering and diffraction of P and SV waves by 'realistic' geometries are studied. The model used for this purpose represents an idealized cross section 0A through the Los Angeles Basin as shown in Figs 7 and 8. The results for this are obtained by assuming the shear wave velocities 2.0 km/sec and 4.6 km/sec for the alluvium layer and the half-space respectively. The longitudinal wave velocities in these two media are chosen to be 3.75 km/sec and 8.3 km/sec respectively. The material density of the alluvium layer is assumed to be 2.25 gm/cc and the density of the half-space material is 2.9 gm/cc. The normalized wave numbers and the normalized rigidity are the given by $K_1/K = 2.3$, $h_1/h = 2.2$ and $\mu_1/\mu_2 = 0.144$.

2.5.1 Displacement amplitudes on surface

Consider first the amplification of P-waves by the idealized sedimentary basin shown by solid line in Fig. 8. The horizontal and vertical surface displacement amplitudes, $|u_x|$ and $|u_y|$, are plotted versus normalized distance x/a_1 for $\eta = 0.5$ and 1.0 in Figs 9 and 10. In each figure the effects of the angle of incident waves $\delta = 85°$, 60°, 30° and 5° are shown. Note that for the assumed

material properties the free field amplitudes for P-waves are

$$|u_x^{ff}| = 0.206 \qquad |u_y^{ff}| = 1.99 \qquad \text{for } \delta = 85°$$

$$|u_x^{ff}| = 1.056 \qquad |u_y^{ff}| = 1.705 \qquad \text{for } \delta = 60°$$

$$|u_x^{ff}| = 1.618 \qquad |u_y^{ff}| = 1.030 \qquad \text{for } \delta = 30°$$

$$|u_x^{ff}| = 0.853 \qquad |u_y^{ff}| = 0.368 \qquad \text{for } \delta = 5°$$

so that the deviation of the amplitudes caused by the inhomogeneous cross section under consideration can be judged relative to those.

The dependence of the displacement amplitudes on the dimensionless frequency η, the geometrical shape of the subsurface inhomogeneities, and the incident angle of the longitudinal P-waves can be seen from these figures. For the higher values of η, shorter wavelength, the amplification patterns are more complex and in some cases the amplitudes almost seven times the free-field amplitude occur, e.g., Fig. 10.

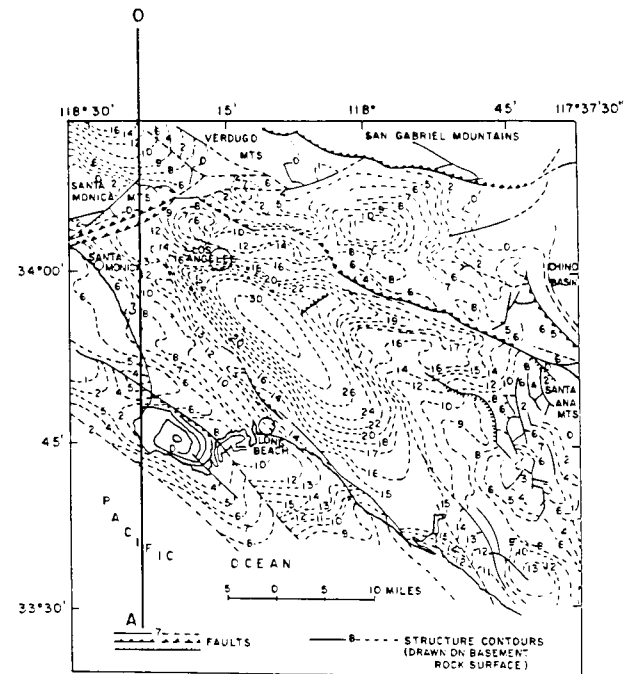Figs 11 and 12 illustrate the amplification patterns induced by SV-waves. Four angles of incidence, $\gamma = 85°$,

Fig. 7. Thickness of alluvium in the vicinity of Los Angeles (after Yerkes et al.[43])
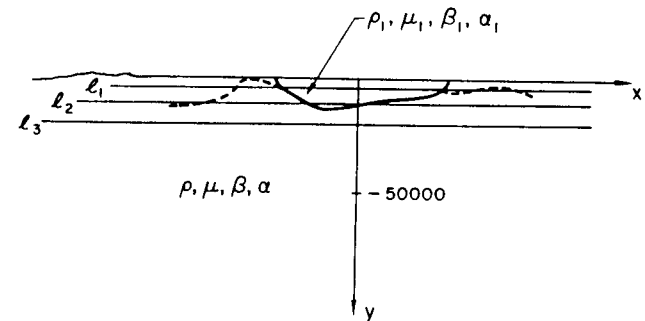

Fig. 8. Typical simplified cross-section (solid line) of sediments in the Los Angeles basin along profile 0A, and the buried horizontal lines l_1, l_2 and l_3
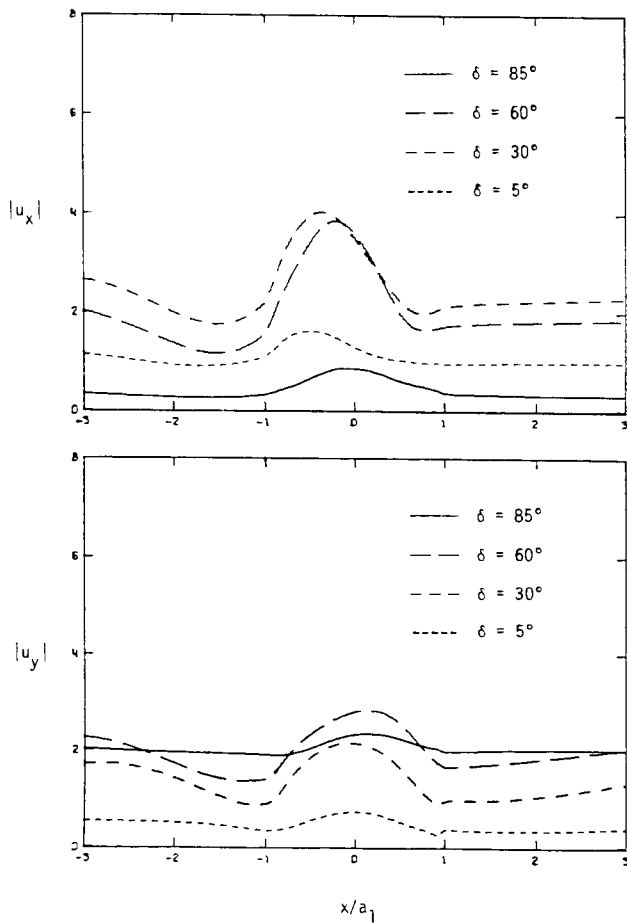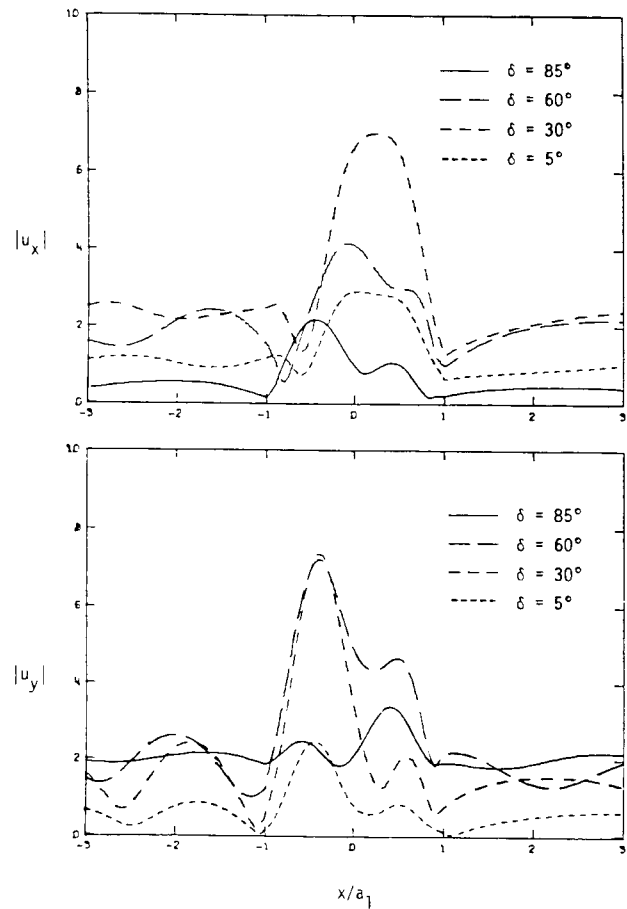
Fig. 9. Horizontal (top) and vertical (bottom) surface displacement amplitudes for cross-section of profile 0A for incident P-waves ($\eta = 0.5$, $K_1/K = 2.3$, $h_1/h = 2.2$, $\mu_1\mu = 0.144$)

Fig. 10. Horizontal (top) and vertical (bottom) surface displacement amplitudes for cross-section of profile 0A for incident P-waves ($\eta = 1.0$, $K_1/K = 2.3$, $h_1/h = 2.2$, $\mu_1/\mu = 0.144$)

$60°$, $30°$ and $5°$ are used for each dimensionless frequency. With critical angle of incidence, $\gamma_{cr} = 56°20'32''$, two of the considered incident angles are beyond the critical angle and the other two are below this angle. The plots represent the surface displacement amplitudes as a function of x/a_1 for values of $\eta = 0.5$ and 1.5. Since the wavelength of SV waves is shorter than that of P waves at the same frequency, the presence of the inhomogeneities can be felt more readily by the SV waves and the diffraction patterns become more complicated for the same η. As a basis for relative comparison of the observed amplitudes, the free-field amplitudes for SV-wave incidence in a uniform half-space are as follows

$$|u_x^{ff}| = 1.977 \qquad |u_y^{ff}| = 0.206 \qquad \gamma = 85°$$

$$|u_x^{ff}| = 1.955 \qquad |u_y^{ff}| = 1.03 \qquad \gamma = 60°$$

$$|u_x^{ff}| = 0.498 \qquad |u_y^{ff}| = 0.956 \qquad \gamma = 30°$$

$$|u_x^{ff}| = 0.170 \qquad |u_y^{ff}| = 0.294 \qquad \gamma = 5°$$

As it can be seen from these figures, the amplification of SV waves by the cross section under study is less than four times that of the free-field.

2.5.2 Displacement amplitudes along buried horizontal lines

The horizontal lines l_1, l_2 and l_3, in Fig. 8 at depths $d = a_1/8$, $a_1/4$ and $a_1/2$ below surface are next considered to

illustrate the displacement amplitudes along the buried lines for the cross section taken from section 0A in Fig. 7 and for incident P and SV waves. Figs 13 and 14 present the displacement amplitudes for P-wave excitation and Figs 15 and 16 show the plots of these amplitudes for incident SV-wave versus the normalized distance x/a_1. Two angles of incidence $30°$ and $60°$ and two values of dimensionless frequency $\eta = 0.5$, and 1.5 are considered in the illustration of these results.

Once again, the dependence of the amplification patterns on the angle of incidence of the incoming wave and on the dimensionless frequency can be seen from these results. The influence of the inhomogeneity tends to decrease as the depth of the buried lines increases. This is more so for smaller values of η, i.e. longer wavelengths. However, localized focussing of wave motion can lead to large amplification of motions for certain geometries of the alluvial valleys and for certain depths d. The occurrance of large amplifications is governed by the direction of wave arrival and by the details of the geometry of each inhomogeneity and thus cannot be predicted in general. Numerous plots presented by Moeen-Vaziri and Trifunac[11] can illustrate this point.

CONCLUSIONS

The problem of the scattering and diffraction of plane waves through two dimensional subsurface irregularities
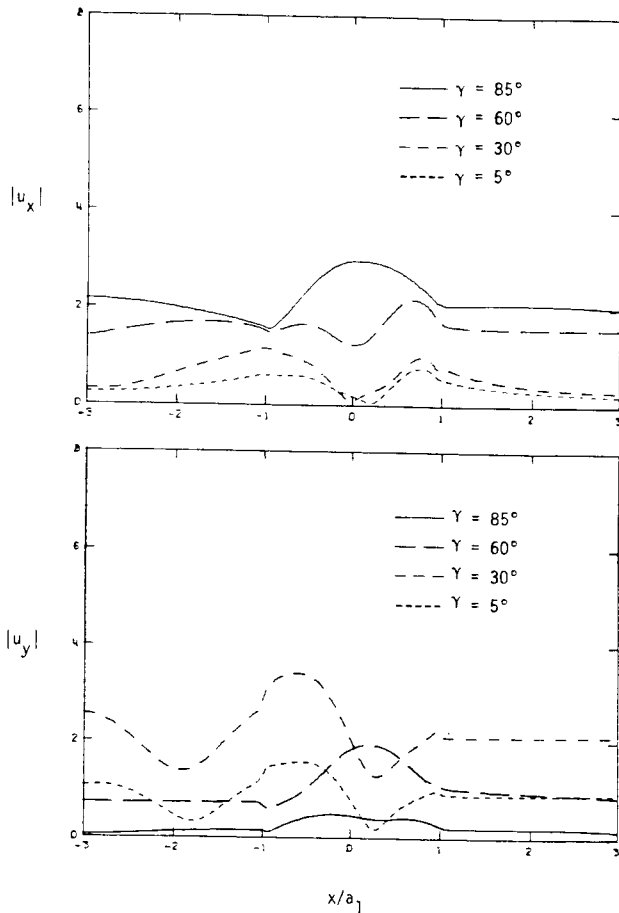
Fig. 11. Horizontal (top) and vertical (bottom) surface displacement amplitudes for cross-section of profile 0A for incident SV-waves ($\eta=0.5$, $K_1/K=2.3$, $h_1/h=2.2$, $\mu_1/\mu=0.144$)
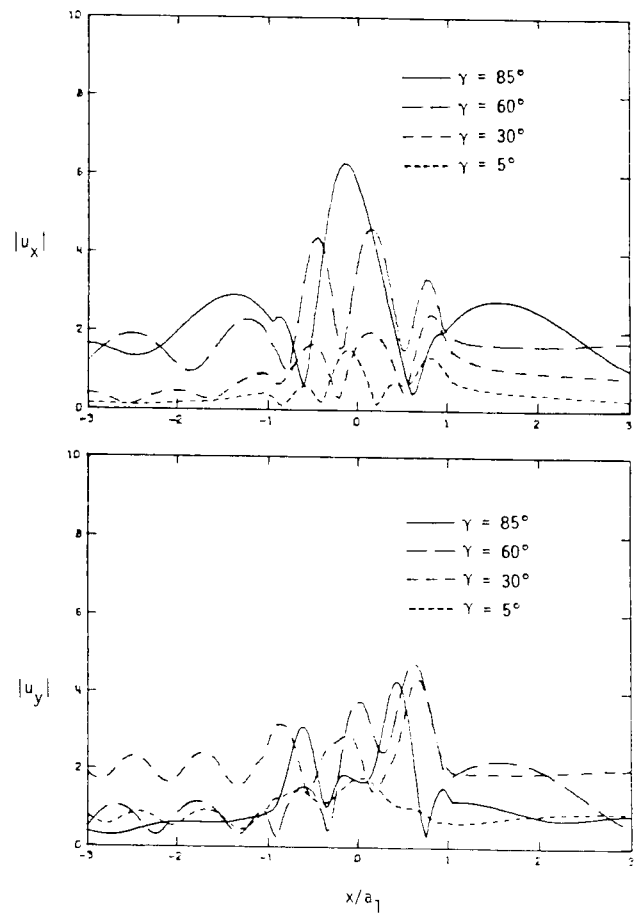

Fig. 12. Horizontal (top) and vertical (bottom) surface displacement amplitudes for cross-section of profile 0A for incident SV-waves ($\eta=1.5$, $K_1/K=2.3$, $h_1/h=2.2$, $\mu_1/\mu=0.144$)

has been investigated. An approximate method which involves series expansions in terms of cylindrical wave functions and a least squares technique have been employed to solve this problem numerically. Throughout the numerical calculations, it was observed that difficulties may arise when the boundaries of the inhomogeneous layers deviate considerably from a circle and for high values of η. For these cases, a greater number of terms in the series of wave functions is needed. However, increasing the number of these terms leads to ill-conditioning and instability of the matrix equations under study. For the incident P and SV waves, the comparisons have been made through constructing a solution in a uniform half-space. The results obtained in this case are in good agreement with those found using an exact solution.

An idealized cross-section of the Los Angeles basin has been chosen to illustrate the effects of more realistic subsurface inhomogeneities on the scattering and diffraction of P and SV waves. Examples of the displacement amplitudes on the surface and along three buried horizontal lines have been presented. For incident P and SV waves the components of these amplitudes along the horizontal, x, and vertical, y, directions were obtained. Different angles of incidence and different values of dimensionless frequency were considered. The amplification patterns are significantly influenced by the

incident angle of the incoming waves, their frequency, and by the geometrical shape of the irregularities.

For waves with shorter wavelengths the amplification patterns are more complex compared to those for waves with long wavelengths. The surface displacement amplitudes may change rapidly from point to point for these short wavelengths. For incident P and SV waves, the amplification factors at ground surface as high as seven and four respectively have been observed.

The interference of waves may lead to a nearly-standing wave pattern at some locations on the surface of the inhomogeneities. The motion at these locations is almost zero. The influence of the subsurface irregularities tends to decrease as the depth of the buried horizontal lines increases.

The application of the foregoing harmonic analysis to transient earthquake excitations is straightforward. Using the harmonic solutions in the frequency domain, the effects of subsurface inhomogeneities can be examined through Fourier synthesis and analysis (Moeen-Vaziri and Trifunac[11]).

REFERENCES

1   Hudson, D. E. Local Distribution of Strong Earthquek Ground Motions, *Bull. Seism. Soc. Amer.*, 1972, **62**, 1765–1786
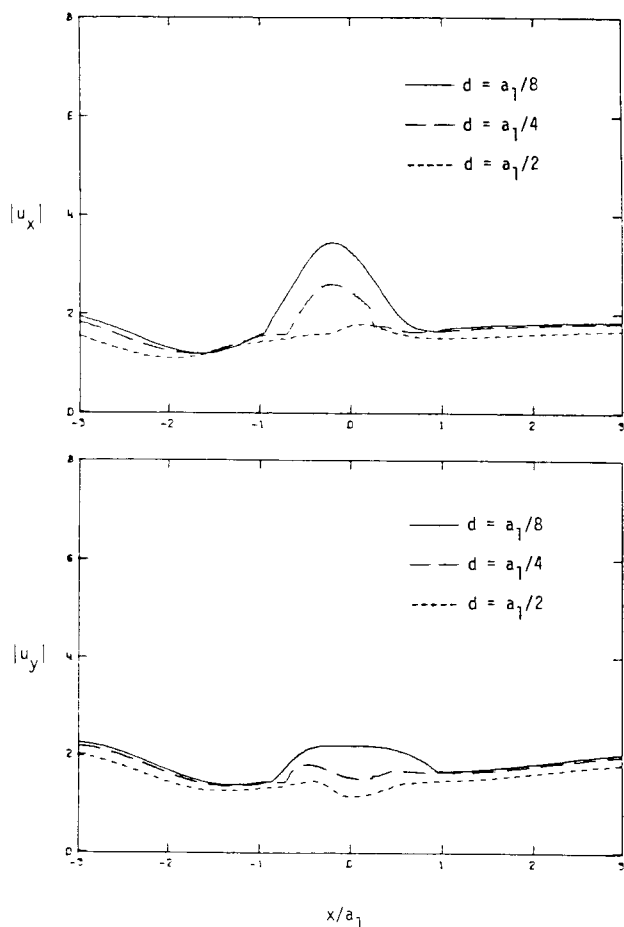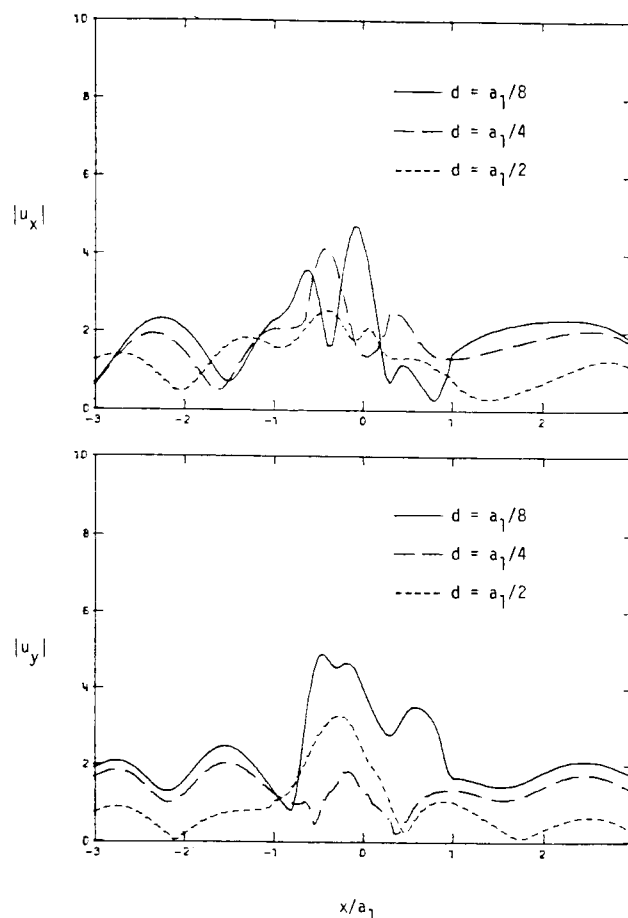
Fig. 13. Horizontal (top) and vertical (bottom) displacement amplitudes along three buried horizontal lines for cross-section of profile 0A for incident P-waves ($\delta = 60°$, $\eta = 0.5$, $K_1/K = 2.3$, $h_1/h = 2.2$, $\mu_1/\mu = 0.144$)

Fig. 14. Horizontal (top) and vertical (bottom) displacement amplitudes along three buried horizontal lines for cross-section of profile 0A for incident P-waves ($\delta = 60°$, $\eta = 1.5$, $K_1/K = 2.3$, $h_1/h = 2.2$, $\mu_1/\mu = 0.144$)

2 Gutenberg, B. Effects of Ground on Earthquake Motion, *Bull. Seism. Soc. Amer.*, 1957, **47**, 221–250

3 Sezawa, K. Scattering of Elastic Waves and Some Allied Problems, *Bull. of Earthquake Res. Inst.*, Tokyo Univ., 1927, **3**, 18

4 Miklowitz, J. Elastic Wave Propagation, Reprinted from Applied Mechanics Survey, Spartan Books, Washington DC, 1966

5 Aki, K. and Larner, K. L. Surface Motion of a Layered Medium having an Irregular Interface due to Incident Plane SH-Waves, *J. Geophys. Res.*, 1970, **75**, 933–954

6 Bard, P. Y. and Bouchon, M. The Seismic Response of Sediment-Filled Valleys. Part 1, The Case of Incident SH-Waves, *Bull. Seis. Soc. Amer.*, 1980, **70**, 1263–1286

7 England, R., Sabina, F. J. and Herrera, I. Scattering of SH-Waves by Superficial Cavities of Arbitrary Shape Using Boundary Methods, *Communicaciones Técnicas*, 1978, **9**

8 Lee, V. W. and Trifunac, M. D. Stresses and Deformations Near Circular Underground Tunnels Subjected to Incident SH-Waves, *ASCE, EMD*, 1979, **105**, 643–659

9 Moeen-Vaziri, N. and Trifunac, M. D. A Note on the Vibrations of a Semi-Circular Canal Excited by Plane SH-Wave, *Bull. ISET*, 1981, **18**, 88 100

10 Moeen-Vaziri, N. and Trifunac, M. D. Scattering of Plane SH-Waves by Cylindrical Canals of Arbitrary Shape, *Int. J. Soil Dyn. and Earthquake Eng.*, 1984, **4**, 18–23

11 Moeen-Vaziri, H. and Trifunac, M. D. Investigation of Scattering and Diffraction of Plane Seismic Waves through Two-Dimensional Inhomogeneities, University of Southern California, Dept. of Civil Engineering Report No. 86-03, 1986

12 Sabina, F. J. and Willis, J. R. Scattering of SH-Waves by a Rough Half-Space of Arbitrary Shape, *Geophysical Journal*, 1975, **42**, 685–703

13 Sánchez-Sesma, F. J. and Esquivel, J. A. Ground Motion on Alluvial Valleys under the Incident Plane SH-Waves, *Bull. Seism. Soc. Amer.*, 1979, **69**, 1107–1120

14 Sáchez-Sesma, F. J. and Rosenblueth, E. Ground Motion at Canyons of Arbitrary Shape Under Incident SH-Waves, *Earthquake Eng. and Struct. Dyn.*, 1979, **7**, 441–450

15 Sánchez-Sesma, F. J., Herrera, I. and Avilés, J. A Boundary Method for Elastic Wave Diffraction: Application to Scattering of SH-Waves by Surface Irregularities, *Bull. Seism. Cos. Amer.*, 1982, **72**, 473–490

16 Sills, L. B. Scattering of Horizontally Polarized Shear Waves by Surface Irregularities, *Geoph. J.R. Astr. Soc.*, 1978, **54**, 319–348

17 Trifunac, M. D. Surface Motion of a Semi-Cylindrical Alluvial Valley for Incident Plane SH Waves, *Bull. Seism. Soc. Amer.*, 1971, **61**, 1755–1770

18 Trifunac, M. D. Scattering of Plane SH Waves by a Semi-Cylindrical Canyon, *Earthquake Eng. and Struct. Dyn.*, 1975, **1**, 267–281

19 Wong, H. L. and Jennings, P. C. Effects of Canyon Topography on Strong Ground Motion, *Bull. Seism. Soc. Amer.*, 1975, **65**, 1239–1257

20 Wong, H. L. and Trifunac, M. D. Scattering of Plane SH Waves by a Semi-Elliptical Canyon, *Earthquake Eng. and Struct. Dyn.*, 1974a, **3**, 157–169

21 Wong, H. L. and Trifunac, M. D. Surface Motion of a Semi-Elliptical Alluvial Valley for Incident Plane SH Waves, *Bull. Seism. Soc. Amer.*, 1974b, **64**, 1389–1408

22 Wong, H. L., Trifunac, M. D. and Westermo, B. Effects of Surface and Subsurface Irregularities on the Amplitudes of Monochromatic Waves, *Bull. Seism. Soc. Amer.*, 1977, **67**, 353–368

23 Cisternas, A., Betancourt, O. and Leiva, A. Body Waves in a Real Earth, Part I, *Bull. Seism. Soc. Amer.*, 1973, **63**, 145–156
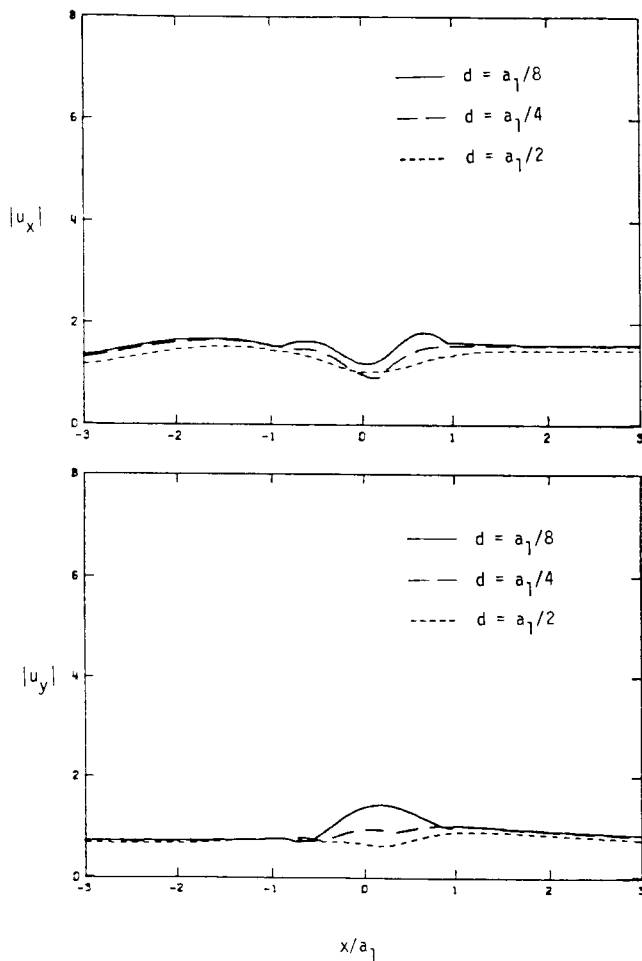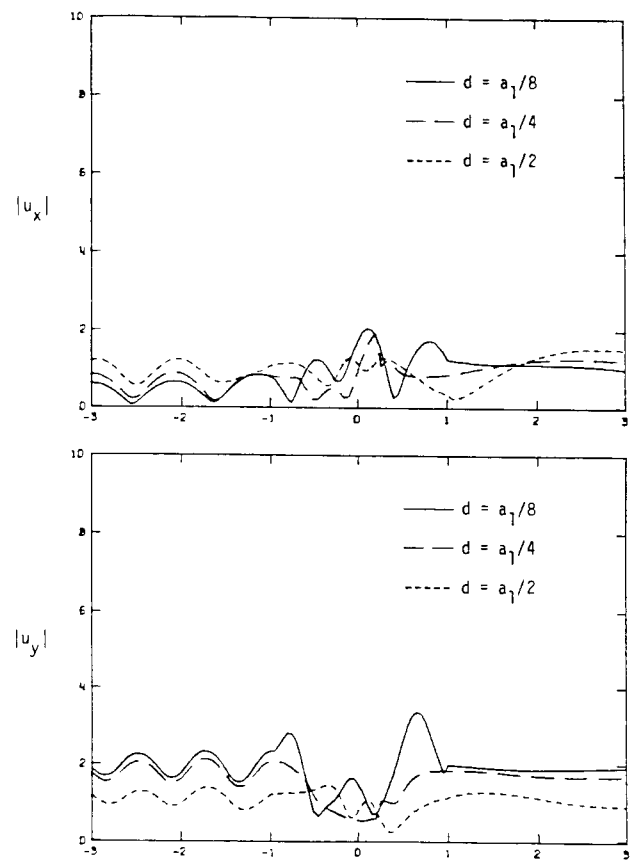
x/a_1

Fig. 15. Horizontal (top) and vertical (bottom) displacement amplitudes along three buried horizontal lines for cross-section of profile $0A$ for incident SV-waves $(\gamma=60°, \eta=0.5, K_1/K=2.3, h_1/h=2.2, \mu_1/\mu=0.144)$

Fig. 16. Horizontal (top) and vertical (bottom) displacement amplitudes along three buried horizontal lines for cross-section of profile $0A$ for incident SV-waves $(\gamma=30°, \eta=1.5, K_1/K=2.3, h_1/h=2.2, \mu_1/\mu=0.144)$

24   Bouchon, M. and Aki, K. Near Field of a Seismic Source in a Layered Medium with Irregular Interfaces, *Geoph. J.R. Astr. Soc.*, 1977, **50**, 669–684

25   Mal, A. K. and Knopoff, L. Transmission of Rayleigh Waves Past a Step Change in Elevation, *Bull. Seism. Soc. Amer.*, 1965, **55**, 319–334

26   Wang, C. Y. and Herrmann, R. B. A Numerical Study of P, SV and SH Wave Generation in a Plane Layered Medium, *Bull. Seism. Soc. Amer.*, 1980, **70**, 1015–1036

27   Bouchon, M. Effect of Topography on Surface Motion, *Bull Seism. Soc. Amer.*, 1973, **63**, 615–632

28   Wong, H. L. Diffraction of P, SV, and Rayleigh Waves by Surface Topographies, University of Southern California, Dept. of Civil Engineering, Report No. CE 79-05

29   Dravinski, M. Influence of Interface Depth Upon Strong Ground Motion, *Bull. Seism. Soc. Amer.*, 1982, **72**, 597–614

30   Dravinski, M. Amplification of P, SV, and Rayleigh Waves by Two Alluvial Valleys, *Soil Dynamics and Earthquake Engineering*, 1983, **2**(2), 66–77

31   McIvor, I. Two-Dimensional Scattering of a Plane Compressional Wave by Surface Imperfections, *Bull. Seism. Soc. Amer.*, 1969, **59**, 1349–1364

32   Asano, S. Reflection and Refraction of Elastic Waves at a Corrugated Surface, *Bull. Seism. Soc. Amer.*, 1966, **56**, 201–221

33   Suteau, A. and Martel, L. Surface Waves in Structures with Locally Irregular Boundaries, *Bull. Seism. Soc. Amer.*, 1980, **70**, 791–808

34   Singh, S. K. and Sabina, F. J. Ground Motion Amplification by Topographic Depressions for Incident P-Wave Under Acoustic Approximation, *Bull. Seism. Soc. Amer.*, 1977, **67**, 345–352

35   Lee, V. W. Diffraction Near a Three-Dimensional Hemispherical Canyon Subjected to Incident Plane Waves, University of Southern California, Dept. of Civil Engineering, Report No. CE 78-16

36   Wong, H. L. Dynamic Soil-Structure Interaction, EERL Report 75-01, Calif. Inst. of Tech., Pasadena, 1975

37   Wong, H. L. and Luco, J. E. Dynamic Response of Foundation of Arbitrary Shape, *Earthquake Eng. and Struct. Dyn.*, 1976, **9**

38   Lee, V. W. and Trifunac, M. D. Body Waves Excitation of Embeded Hemispheres, ASCE, EMD, 1982, **108**, 546–563

39   Sáchez-Sesma, F. J. Diffraction of Elastic Waves by Three-Dimensional Surface Irregularities, *Bull. Seism. Soc. Amer.*, 1983, **74**

40   Achenbach, J. D. Wave Propagation in Elastic Solids, North-Holland, Amsterdam, 1973

41   Pao, Y. H. and Mow, C. C. Diffraction of Elastic Waves and Dynamic Stress Concentrations, Crane, Russak and Company, In., New York, 1973

42   Trifunac, M. D. A Note on Rotational Components of Earthquake Motions on Ground Surface for Incident Body Waves, *Soil Dyn. and Earthquake Eng.*, 1982, **1**, 11–19

43   Yerkes, R. F. McCulloh, Schoellhamer, J. E. and Vedder, J. G. Geology of the Los Angeles Basin, California - an Introduction, US Geological Survey Professional Paper 420-A, 1965